OXFORD JOURNAL
OF STUDENT
SCHOLARSHIP

A Comparative Analysis of Systems for Single-Tile Chess Piece Capture Mechanisms

Atilla Aras Baysal
atillaarasbaysal@gmail.com

ABSTRACT

This research addresses the inefficiency of piece captures in automated chess, where current systems typically use the same mechanism for both standard movement and piece capture, resulting in significantly increased time, energy, and calculation. This study aims to offer a faster alternative by presenting and analysing two novel piece capture mechanisms intended to be integrated into existing automated chessboards. The proposed system is designed to fit under each tile and function as a trapdoor, opening to allow a captured piece to fall into the chessboard's interior while a separate mechanism moves the capturing piece.

Two designs were developed: the coupler-tile and the follower-tile model. They both utilise a combination of four-bar linkages and cam & follower systems to achieve a controlled lift and tilt. The 3D CAD models were created in Autodesk's Fusion v.2604. They were simulated and analysed using Rigid Body Dynamics simulations in ANSYS to evaluate displacement, velocity, acceleration, and joint forces over a 3-second motion. The quantitative analysis confirmed that both designs achieved the intended smooth, non-colliding motion. The follower-tile design was found to be simpler and offer greater mobility, whereas the coupler-tile design, being more complex, showed lower overall forces on its joints, suggesting improved longevity. However, it is noted that these simulations were conducted under idealized conditions, assuming rigid bodies, negligible friction, and constant input speeds. Crucially, the simulation data confirms that the dynamic loads remain well within the capacity of standard manufacturing materials. By rigorously validating kinematic performance and feasibility through the quantitative analysis of both models in a physics-based simulation environment, this study establishes a robust engineering framework. Consequently, the designs serve as simulation-based proofs of concept with hardware validation left to future work.

INTRODUCTION

The automation of chess presents an engineering challenge that bridges the gap between digital and on-board gameplay, compelling researchers to try and balance many aspects such as motion planning and precision mechanics. This unique topic, while seemingly straightforward, requires the consideration of many constraints, and thus, it has been a point of interest of researchers for many years, starting from the infamous "Turk" (one of the first designs that had claimed to automate the chessboard and include a computer opponent, though later revealed to be a fraud). Such a creation not only adds to the intellectual entertainment sought by chess hobbyists, but can also be the sole way of enjoying this refined game for physically impaired individuals.

Papers on this subject typically discuss two methods of chess piece movement. One method uses a robotic arm that fixes on pieces via either a magnet or a clamping mechanism. Servo motors on the multiple joints of said arms make for a system that has a very high degree of freedom. In turn, the great number of possibilities of moves slows the calculation speed while also increasing cost and fragility. For example, Ómarsdóttir et al. [1] developed a robotic arm that uses magnets to attach to chess pieces, placing captured pieces into a separate "graveyard" bin. Similarly, Truong Duc Phuc et al. [2] designed an autonomous chess robot that relies on computer vision and deep learning to perform moves. In their system, a simple move takes approximately 20 seconds, a capture move about 60 seconds, and a pawn promotion roughly 90 seconds, as the robot must pick up the captured piece, place it in the storage box, and then retrieve and position the desired piece. Another study by Shin et al. [1] explored the capabilities of a general usage 6-DOF robotic arm. Along with their optimised algorithm for board scanning, a move took 26.8 s on average. More recently, Zhang et al. [2] employed a 7-DOF robotic arm for the automation of chess. Their study mentions an average of 6.24 s for capture moves and an average of 7.33 s for standard moves. The discrepancy was due to some standard moves included jumping over pieces, which increased the average. This literature review suggests that the complexity of robotic arms generally leads to slower moves, higher energy expenditure, and increased fragility, echoing the limitations observed in multi-joint servo systems. Though the study of Zhang et al. is an exception on the move duration aspect, other drawbacks such as substantial computational requirements still apply.

The second common method of piece movement discussed in the literature is the use of magnetic slider mechanisms placed under the board. These mechanisms lift and connect to the piece, slide it to the desired location, and lower down to disconnect. Jariyavajee et al.'s [5] interactive chess board moves captured pieces to a "killed" area located on either side of the board, while Sarker et al.'s Wizard Chess [6] system uses reed switches under the tiles of removed pieces to communicate with the controller board. Thabet et al. [3] used the CoreXY motion system to actuate the pieces, and reported that movements took between 20 and 50 s. A commercial product named *Chessnut Move Advanced Robotic Chessboard* [4] also uses sliders to position the pieces, reportedly capable of simultaneously positioning every piece. The product details mention each move taking less than 3 s. This approach to piece actuation offers relative simplicity, accelerating calculation speed and reducing mechanical stress, though it lacks the multi-dimensional flexibility of a robotic arm. However, this simplicity can be exchanged for speed, such as in the case of *Chessnut*, resulting in very fast movements but also a significantly increased computational load for path

planning. This lack of vertical movement could cause nearby pieces to collide during motion, resulting in pieces deviating progressively from their expected locations in subsequent moves.

To implement the precise movements such as those required in piece capture, various mechanisms have been explored in other domains of engineering. Applying these insights can help optimise robotic arm-driven or slider-based chess systems by balancing flexibility, robustness, and computational efficiency. A 4-bar linkage system offers a high degree of variability, robustness, and computational simplicity. Kashef et al. [9] proposed a robot hand structure using a four-bar linkage mechanism to improve durability and motion accuracy over cable-driven designs, while Truong et al. [10] demonstrated that four-bar mechanisms can amplify flapping angles in compliant actuators. On the other hand, a cam & follower system offers superior manoeuvrability along a single axis. Mali et al. [11] highlighted its widespread application in internal combustion engines and other automated machinery, and Prasad et al. [12] analysed how cam-follower mechanisms can reduce jerk and induced stresses. These examples from broader engineering illustrate the trade-offs between multi-axis flexibility, robustness, and computational ease, providing insight into which mechanisms could optimise automated chess movement.

Despite the mentioned engineering advances being applicable in the automation of chess piece captures, the research done on chessboard automation has not introduced piece capture mechanisms differing from piece movement mechanisms. Because existing literature focuses heavily on piece actuation and the necessary software, the possible applications of these mechanisms in the context of captures were never explored. As a direct result, capture moves take significantly more time than standard moves, as the movement mechanism must remove the captured piece, return, and position the capturing piece. Consequently, these moves require significantly more energy and computational resources.

This research aims to offer an alternative to the limitations of current approaches by presenting two novel mechanisms that can be integrated into existing methods: the coupler-tile and the follower-tile. These mechanisms combine 4-bar linkages and cam & follower systems and are positioned beneath each tile, raising and tilting the surface to allow the piece to fall into the chessboard and be captured. A simulation-based evaluation framework that measures kinematic performance as well as joint reaction forces during the defined 3 second cycle was established. The analysis revealed that while the follower-tile offers greater range of motion with fewer hardware components, the coupler-tile shows lower peak joint forces that favour longevity. While this approach increases the hardware complexity of existing systems, it eliminates the computational load and the time requirements of extra path-planning needed for capture moves. Finally, this study is positioned as a proof of concept, making modelling assumptions explicit and outlining integration, actuation, and collection considerations to support future prototyping.

METHODS

3.1 Design Description

This study aims to explore the aforementioned lack of capture-dedicated mechanisms on an automated chessboard. The proposed mechanisms would be inserted under each tile. These mechanisms would open, similar to trapdoors, each letting the piece above it to fall into the chessboard itself. This would enable the capture to occur whilst another mechanism, such as a robotic arm, would move the capturing piece to the designated location.

This study therefore examines two mechanisms combining four-bar linkages with cam & follower systems to achieve the controlled lifting and tilting of a single chess tile. The envisioned systems for this tile manipulation needed to be capable of both a rising motion and slanting capabilities. A model simple enough to fit under the board and solely constituting 4-bar linkages was therefore inadequate, as the tile was unable to tilt without colliding with adjacent tiles that were level with it in the initial position. Similarly, a compact model utilizing only cam and follower systems lacked the manoeuvrability, as it could tilt the tile but not while creating an opening for the piece to fall into. Therefore, the final designs combine the range of motion that a 4-bar linkage offers with the precise lift of a cam system. The dimensions of the chess tile were chosen accordingly, measuring 40 mm on each side, to allow for easy integration of the mechanical parts. The 3D CAD designs were all made in the Autodesk's Fusion v.2604 program.

Assumptions & Modelling Scope

For visual clarity, *Figures 1-4* omit guide rails, which would restrict the movement of the frames to the vertical axis, and supports, which would keep the structures stable. Additionally, translational joints that bear no load were defined within the simulation to constrain the direction of the frame movement. These simplifications were made after ensuring that no quantitative data would be lost during the analysis. Models that are fully supported are provided in *Figure 5*. However, electrical components are not depicted, as the scope of this study is limited to the mechanical design and kinematic analysis.

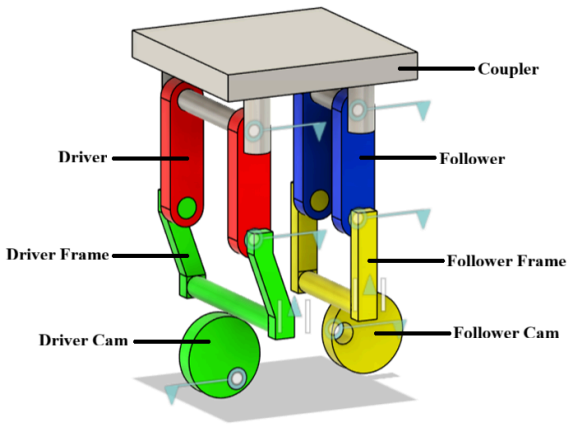

Figure 1 depicts the coupler-tile design, the primary components of the system labelled. This system is designed to be equipped under each tile of an automated chessboard. The tile (the coupler) would tilt owing to the motion created by servos placed on the driver-driver frame, the driver cam, and the follower cam joints.

In *Figure 1*, the coupler-tile design is shown. This design consists of two drivers, coloured red, one coupler, coloured grey, two followers, coloured blue, one driver and one follower frame, green and yellow respectively, and one driver and one follower cam, having the same colours as their frames. The modelling choices were made for the following reasons: The drivers were placed further apart than the followers, allowing them to tilt without collision between machine parts and to avoid the falling piece owing to the gap. The shape of the driver frame was chosen as such because having a base further than the opening of the tile allowed the chess piece to avoid impacting and getting stuck on the mechanisms.

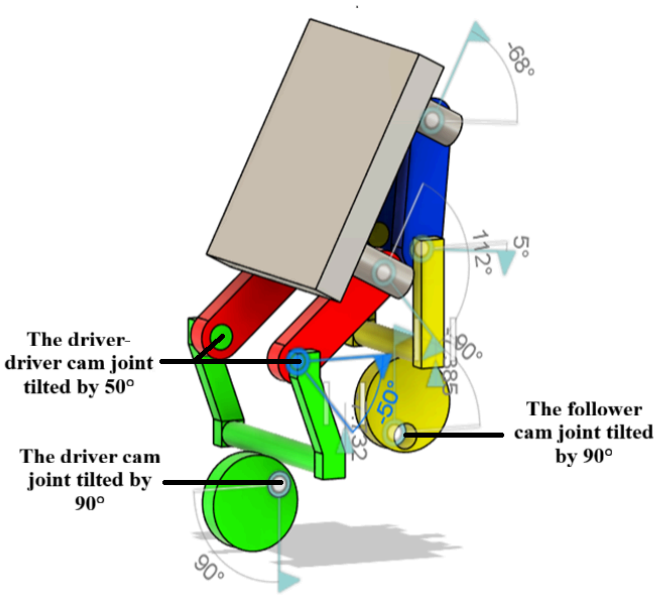

Figure 2 depicts the coupler-tile design in its actuated position. The labels show the actuation centres with their corresponding angular values. Note that the components labelled in Figure 1 correspond to those in Figure 2.

The motion of this design resulting in *Figure 2*, the opening of the tile, is driven by three joints. The follower frame is raised, owing to its cam's 90° of actuation, allowing the tilt to occur without colliding with the adjacent tiles. Meanwhile, the driver frame is lowered by its cam's 90° of actuation, increasing the possible tilt of the tile by 23.1°. This was calculated by comparing the situation where only the follower cam and the driver was actuated to the situation where all three were actuated; the case where only the driver was actuated was deemed irrelevant, as the actuation of the driver only displaces the tile while keeping it level. This comparison showed that the actuation done in *Figure 2* created a tilt of 62.5°, while the situation where the driver cam remained unactuated created a tilt of 39.4°. This ratio of

approximately 1.59 indicates that the rotation of the driver cam is essential. Finally, the driver, leaning towards the follower by 50°, completes the opening of the tile.

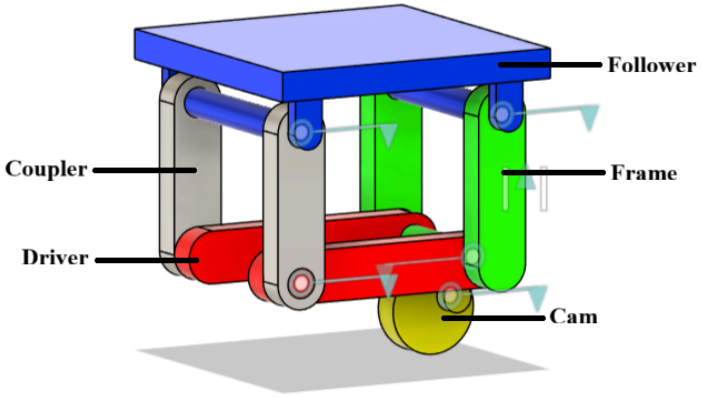

Figure 3 depicts the follower-tile, the primary components of the system labelled. This system is also designed to fit under every tile of an automated chessboard. The tile (the follower) would tilt owing to the motion created by the driver-frame and the cam joints.

In *Figure 3*, the follower-tile design is shown, containing two drivers in red, two couplers in grey, a follower in blue, two frames in green, and a cam in yellow. The difference between the 1.6 cm of distance between the drivers and 2.4 cm for that of the couplers allow the design to fold onto itself without collisions, creating room for the tilt.

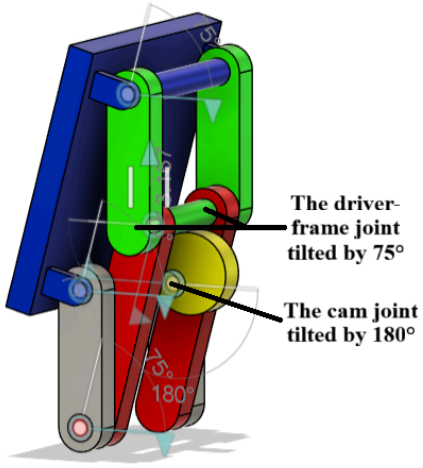

Figure 4 depicts the follower-tile design in its actuated position. The labels show the actuation centres with their corresponding angular values. Note that the components labelled in Figure 3 correspond to those in Figure 4.

Possessing one fewer cam, this model is driven by two joints and resulting opening of the tile is shown in *Figure 4*. The actuation by 180° of the cam joint raises the frame, removing the possibility of a collision between tiles, and the driver-frame joint tilts the driver downwards by 75°, finishing the capture. The absence of a second cam lessens the complexity but puts more load on the driver-coupler and driver frame joints.

Overall, both systems were designed with the intention of producing a smooth lift and tilt. A symmetric and circular cam profile was chosen for this purpose. The equal lengths of drivers and followers and couplers and frames avoid load imbalance and result in a predictable behaviour that can be further modified.

Summary of Designs

	Coupler-tile Design *(Figure 1)*	Follower-tile Design *(Figure 2)*
Drivers	2, red	2, red
Couplers	1, the tile, grey	2, grey
Followers	2, blue	1, the tile, blue
Frames	1 driver frame, green; 1 follower frame, yellow	2 frames, connected by a cylindrical rod, green
Cams	1 driver cam, green; 1 follower cam, yellow	1, yellow
Joints	2 driver-coupler joints, 2 coupler-follower joints, 2 driver-(driver) frame joints, 2 follower-(follower) frame joints, 1 driver cam joint, 1 follower cam joint	2 driver-coupler joints, 2 coupler-follower joints, 2 driver-frame joints, 2 follower-frame joints, 1 cam joint

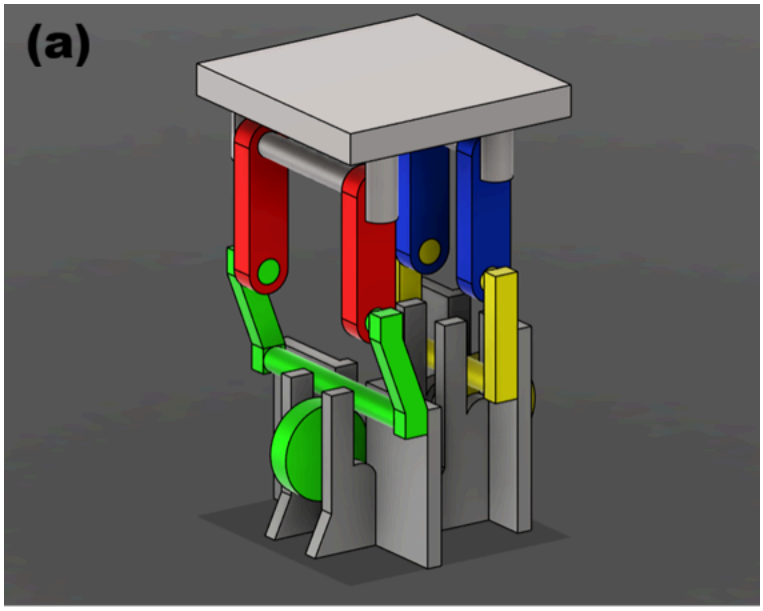
(a)

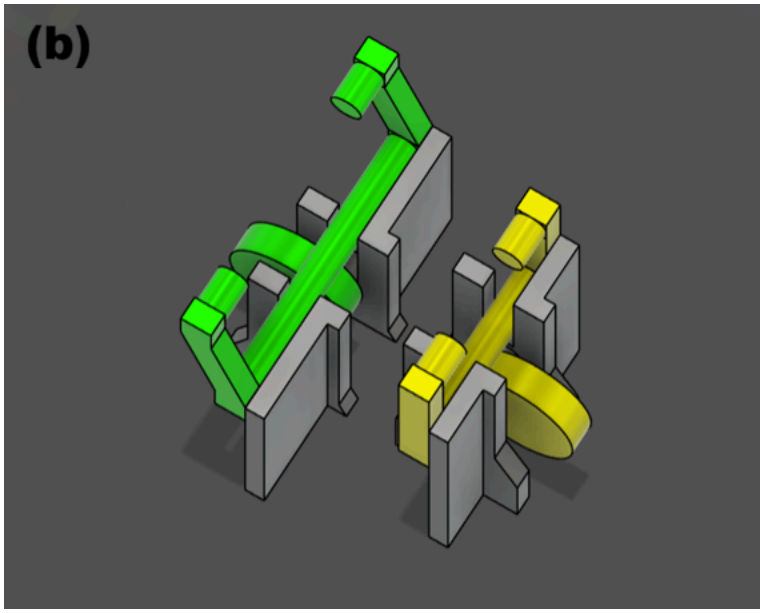
(b)

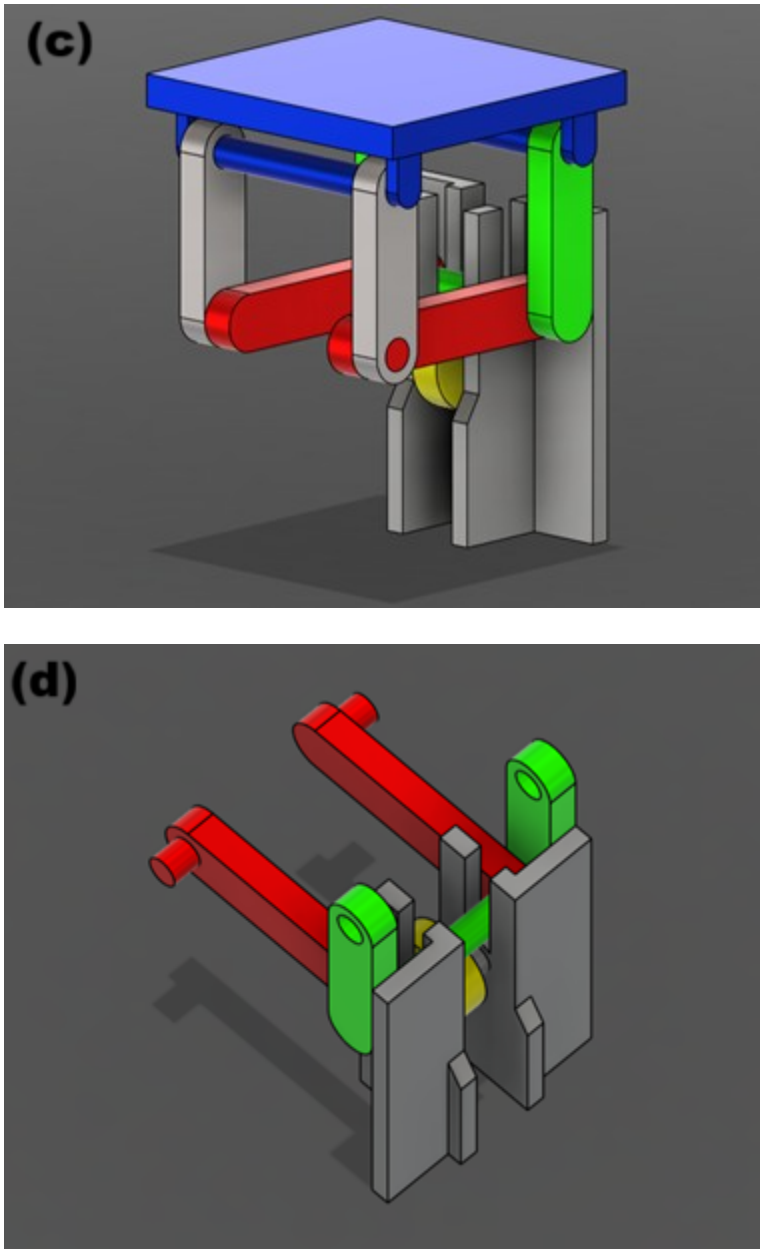

Figure 5 illustrates the comprehensive views of the fully supported capture mechanisms. ***(a)*** *Full assembly of the coupler-tile design.* ***(b)*** *Rear-top view of the coupler-tile design depicting only the driver and follower cams, frames, and their respective supports.* ***(c)*** *Full assembly of the follower-tile design.* ***(d)*** *Rear-top view of the follower-tile design, depicting only the driver, frame, cam, and support.*

Panels **(a)** and **(c)** in *Figure 5* depict the final fully assembled designs created in this paper. The support structures are attached to the base of the chessboard, ensuring structural stability. Both structures are

symmetrical about the plane passing through their cams, and contact the adjacent tiles. This contact, along with the symmetry of the designs, provides resistance to lateral tilting. The driver-frame joints on both models are designed to integrate servo motors, allowing these joints to be actuated or locked in position. Together with the supports, which are clearly visible in the simplified panels **(b)** and **(d)**, the servos ensure frontal stability. As previously mentioned, the electrical systems are excluded from this mechanical analysis.

3.2 Simulation Setup

The models were exported from Autodesk's Fusion v.2604 to ANSYS 2025 R2 as SAT files. This change was made to make use of the Rigid Body Dynamics module of the program, offering detailed analysis of the movements and forces.

Joints were redefined, and joint loads were set for the motion-driving articulations. The coupler-tile design's cams were defined to have a rotational velocity of 30°/s, finishing their motion in 3 seconds as planned. This speed is higher than that of other automated chess captures. This duration was determined to imitate a piece capture move in a real-life chess match. The calculated 50° of tilt that the driver-frame joint was designed to have was also spread to these three seconds, resulting in the rotational speed of 16.67°/s on the driver.

The follower-tile model's driver frame joint was intended to have a rotation of 75°, and its cam was set to have a rotation of 180°. To have comparable results, the same 3 second limit was applied on this design, resulting in the rotational velocities of 25°/s for the driver frame joint and 60°/s for the cam.

The simulations measured the tile's displacement, velocity and acceleration, at a sampling rate of 0.05 s per step, at its centre of mass and at the edge of the tile that tilts open. The global Z-axis represents the vertical direction in this simulation, and all positions are referenced to the global frame. The smoothness of the curve of the velocity and acceleration graphs would indicate that less energy is wasted as vibrations. Curves on the positional graphs showing continuous and smooth displacement towards the required positions would indicate that the mechanisms do not waste energy on redundant movements. Joint forces, magnitudes of the X, Y and Z components, were also collected with the same sampling rate. The low forces on these graphs would show low wear, thus indicating longevity. Overall, these graphs will be used to evaluate the mechanism's efficiency, motion smoothness, and structural reliability.

The obtained graphs were exported to Microsoft Excel for processing and plotting.

3.3 Quantitative Analysis

Plots generated were as follows:

a) Positions

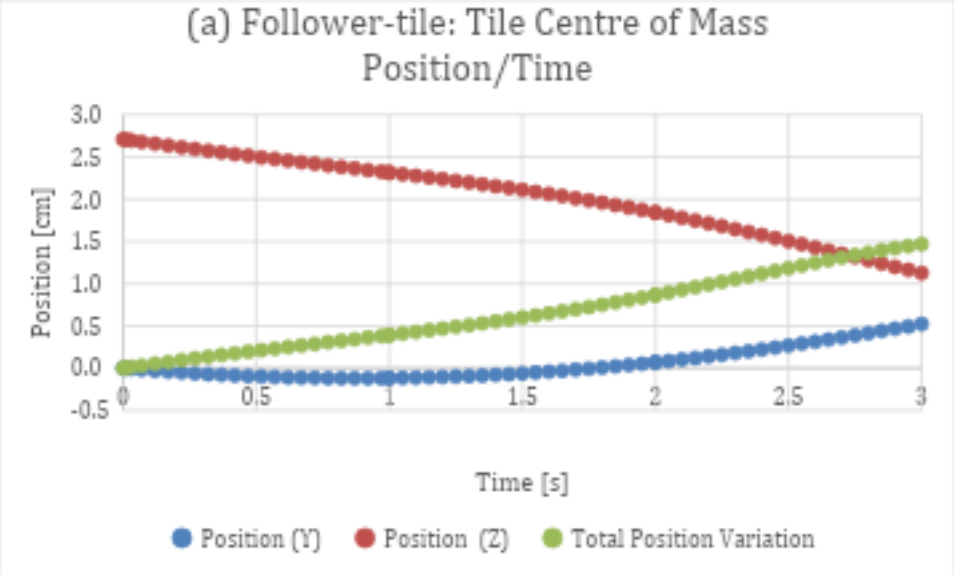

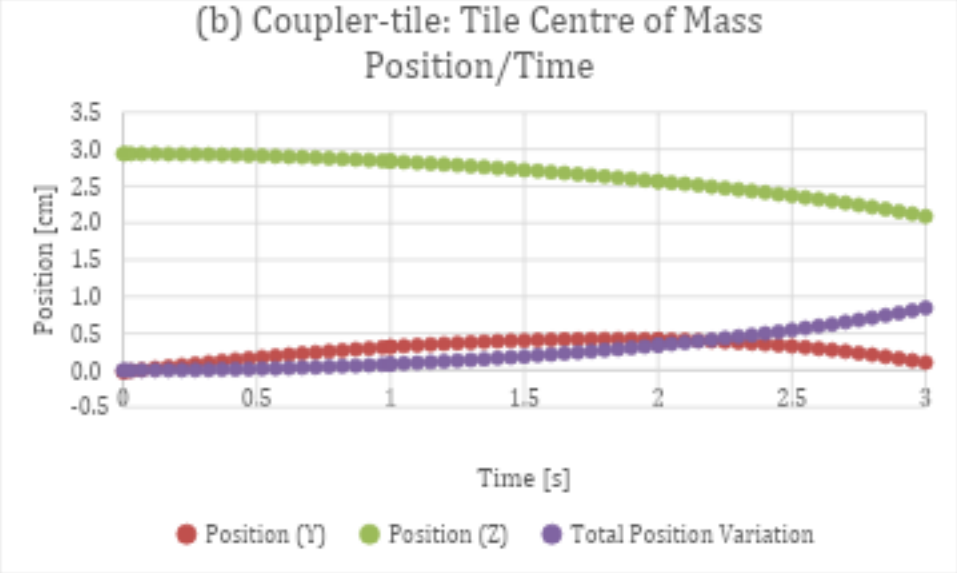

Figure 6 illustrates the position of the tile's centre of mass as a function of time for the two proposed mechanisms. ***(a)*** *The Follower-tile configuration.* ***(b)*** *The Coupler-tile configuration.*

The graphs of positional variations of both centres of mass depicted in *Figure 6* are smooth curves, both reaching the maximum displacement when the tile is in its fully tilted position. The final total

displacement of the follower-tile's centre of mass is approximately 1.5 cm *(a)*, while that of the coupler-tile is under 1 cm *(b)*.

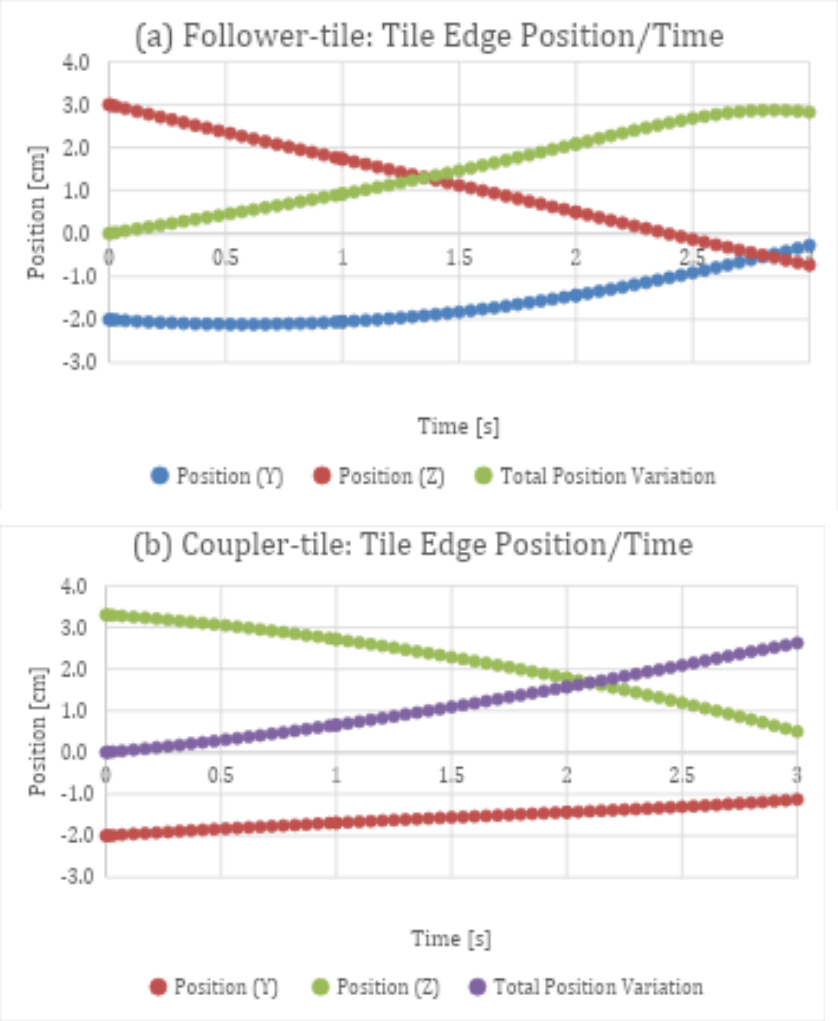

Figure 7 depicts the position of the tile edge as a function of time for the two proposed mechanisms. ***(a)*** *The Follower-tile configuration.* ***(b)*** *The Coupler-tile configuration.*

This trend holds true in *Figure 7* for the edge of the tile that opens as well, and it is worth noting that the largest displacement happened on the Z axis for the follower-tile edge with almost 4 cm *(a)*.

b) Velocity

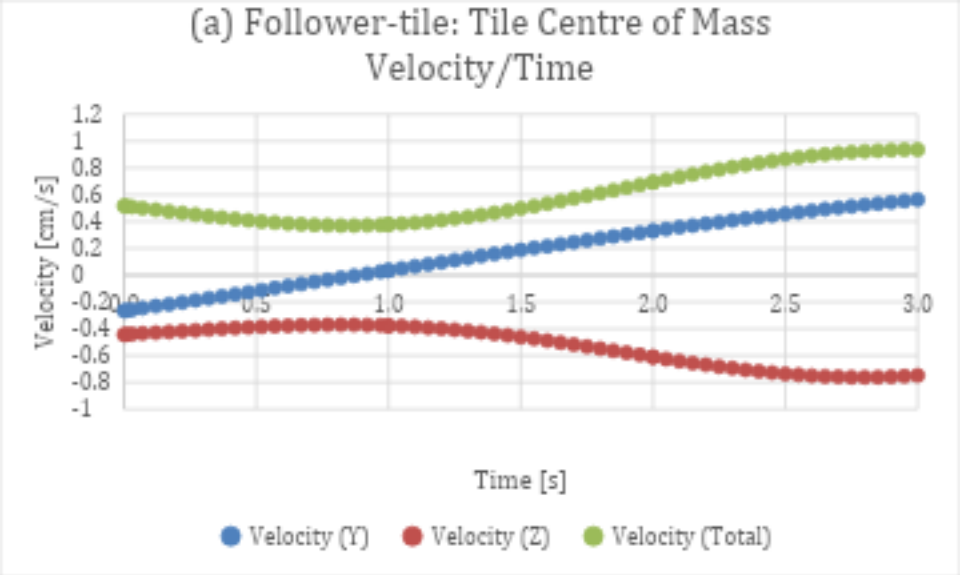
(a) Follower-tile: Tile Centre of Mass Velocity/Time
Velocity [cm/s]
1.2
1
0.8
0.6
0.4
0.2
0
-0.2
-0.4
-0.6
-0.8
-1
0.0
0.5
1.0
1.5
2.0
2.5
3.0
Time [s]
Velocity (Y)
Velocity (Z)
Velocity (Total)

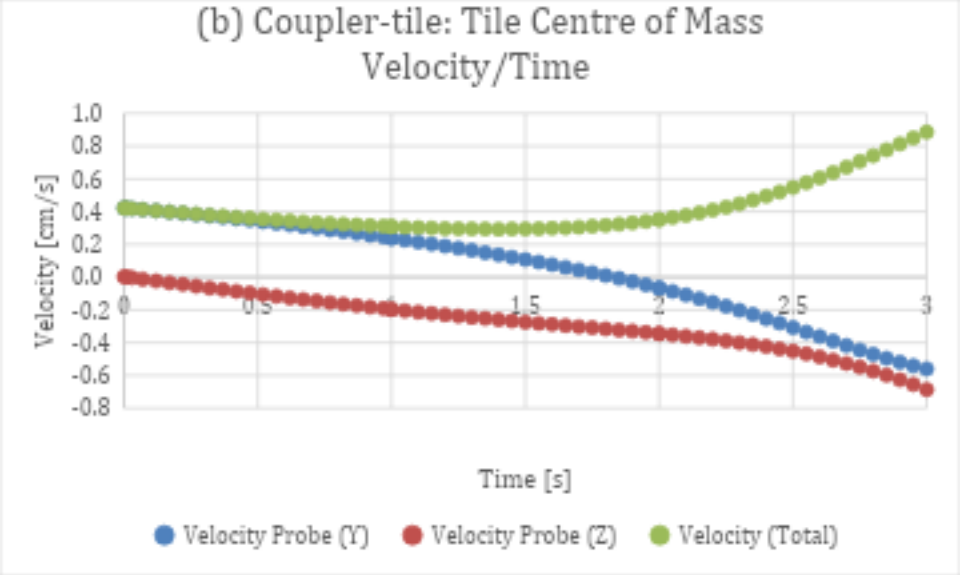
(b) Coupler-tile: Tile Centre of Mass Velocity/Time
Velocity [cm/s]
1.0
0.8
0.6
0.4
0.2
0.0
-0.2
-0.4
-0.6
-0.8
0
0.5
1.5
2
2.5
3
Time [s]
Velocity Probe (Y)
Velocity Probe (Z)
Velocity (Total)

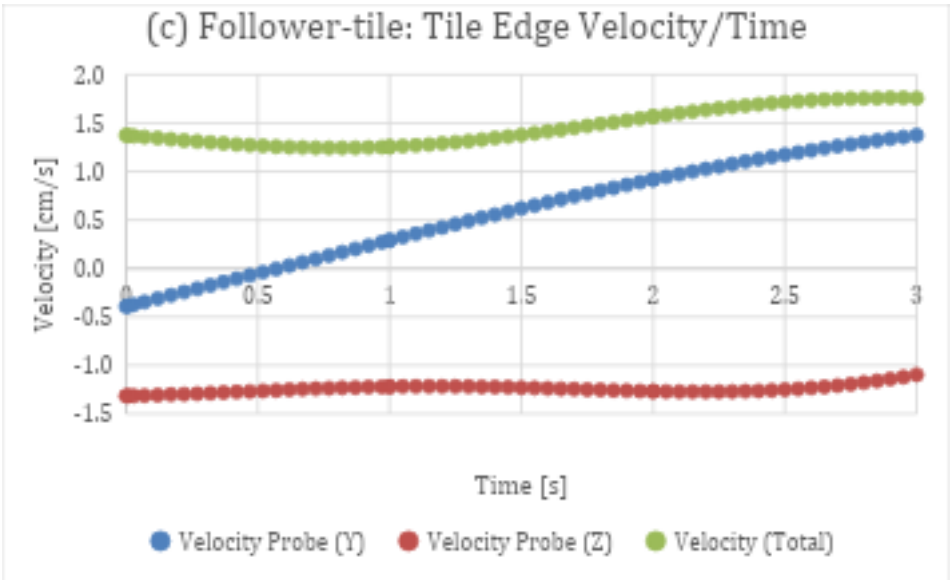

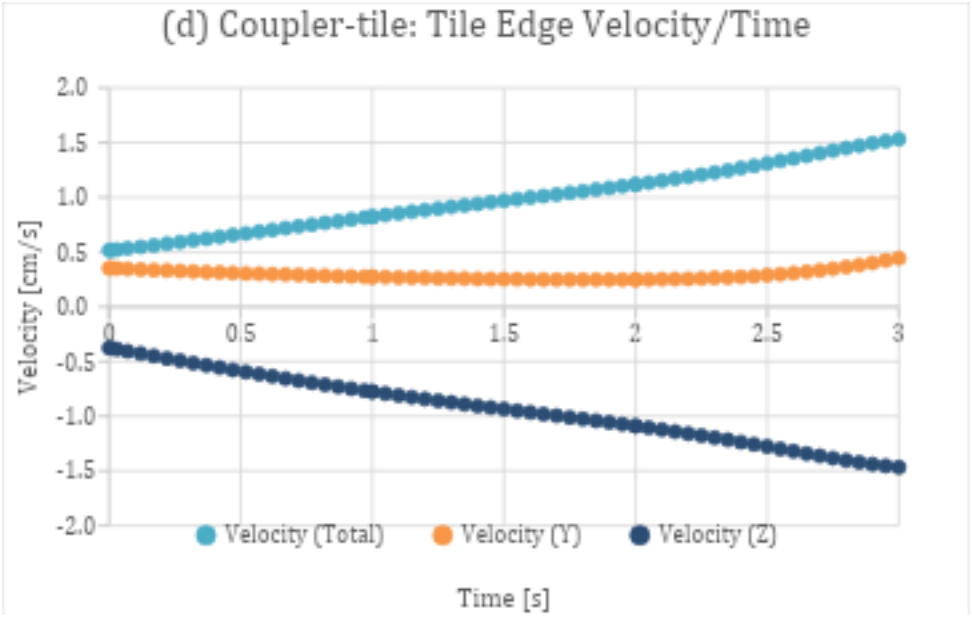

Figure 8 demonstrates velocity profiles of the tile components as a function of time. ***(a)*** *Centre of mass velocity of the Follower-tile configuration.* ***(b)*** *Centre of mass velocity of the Coupler-tile configuration.* ***(c)*** *Tile edge velocity of the Follower-tile configuration.* ***(d)*** *Tile edge velocity of the Coupler-tile configuration.*

The follower-tile's overall velocity is higher than the coupler-tile model's, the speed of its centre peaking at 3 s *(a)* while that of its edge peaks at 2.5 s *(c)*, having relative speeds of 0.95 cm/s and 1.75 cm/s respectively.

Though the centre of mass of the coupler-tile does reach the same highest point of the follower-tile, its speed stays under 0.5 cm/s for more than half of the duration *(b)*. And its total edge speed also lacks behind by measuring 1.5 cm/s at its highest *(d)*.

Overall, smooth curves are observed in Figure 8 and therefore velocities did not have any spikes or discontinuities for the 3 second duration.

c) Acceleration

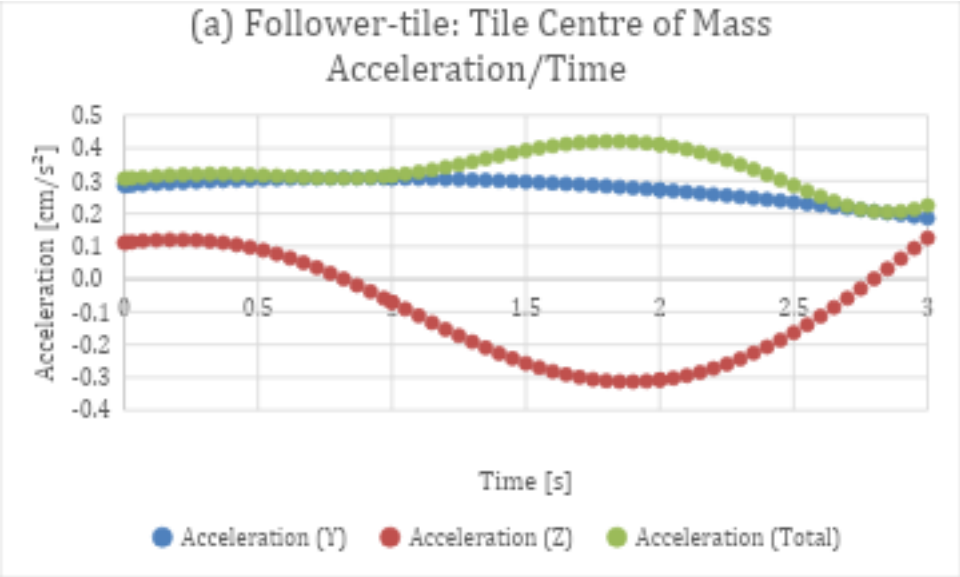

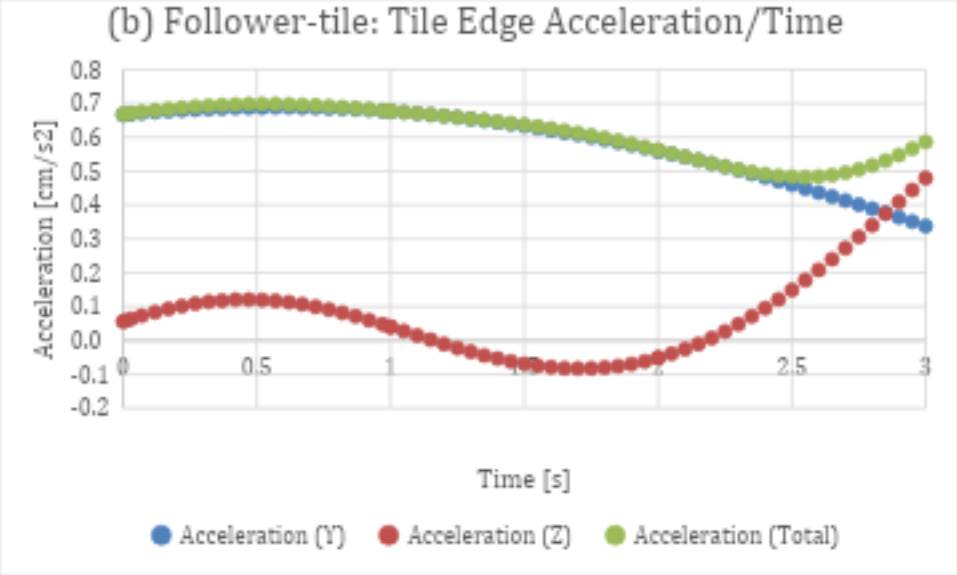

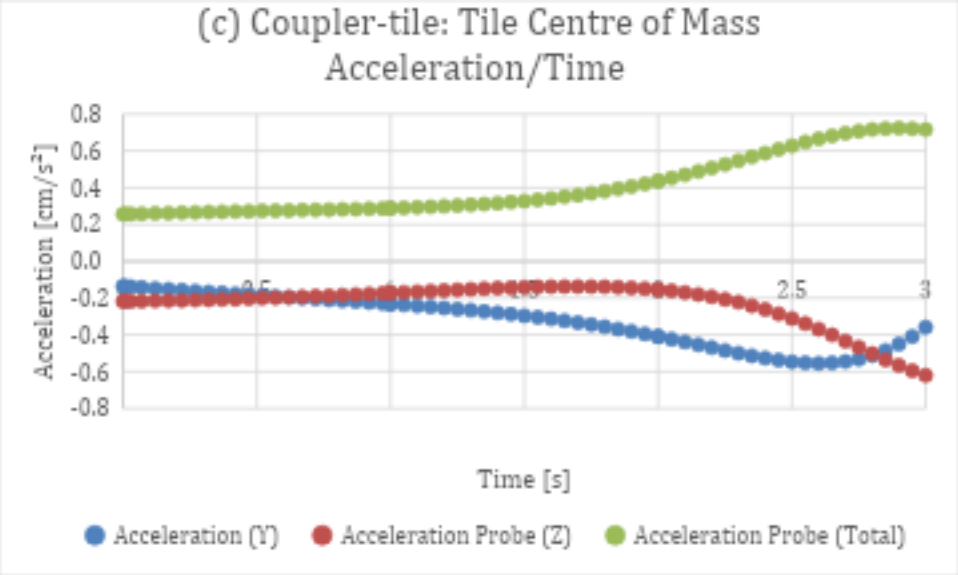

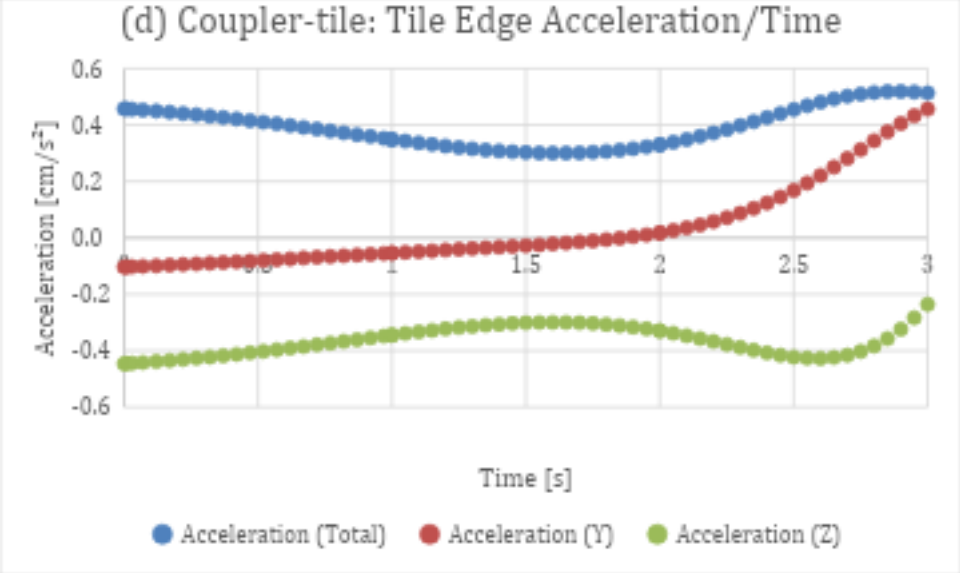

Figure 9 presents acceleration profiles of the tile components as a function of time. ***(a)*** *Centre of mass acceleration of the Follower-tile configuration.* ***(b)*** *Tile edge acceleration of the Follower-tile configuration.* ***(c)*** *Centre of mass acceleration of the Coupler-tile configuration.* ***(d)*** *Tile edge acceleration of the Coupler-tile configuration.*

The total acceleration of the follower-tile's edge dips at 2.5 s, from 0.7 cm/s^2 to 0.5 cm/s^2, then rises when nearing 3 seconds, measuring 0.6 cm/s^2 *(b)*. This rise is because of the spike of acceleration at the z axis, but the inverse happens for the coupler-tile's edge. Its acceleration drops from 0.45 cm/s^2 to 0.3 cm/s^2 at

1.5 s. Afterwards, gaining acceleration on the y axis, its final and maximum acceleration measures 0.5 cm/s^2 *(d)*.

The centre of the follower-tile's acceleration shows similar trends in components to its edge, difference being the former's small magnitude. Starting at 0.3 cm/s^2, the graph stays level until an increase happens in 1 s, peaking at 1.8 s with a value of 0.45 cm/s^2, and later falling back down to 0.2 cm/s^2 *(a)*.

The total acceleration of the coupler-tile's centre mirrors its y-component across the x-axis, differing from that of the follower-tile, which mirrored its z-component. The initial acceleration of 0.25 cm/s^2 increases to 0.7 cm/s^2 at the end *(c)*.

d) Joint Forces

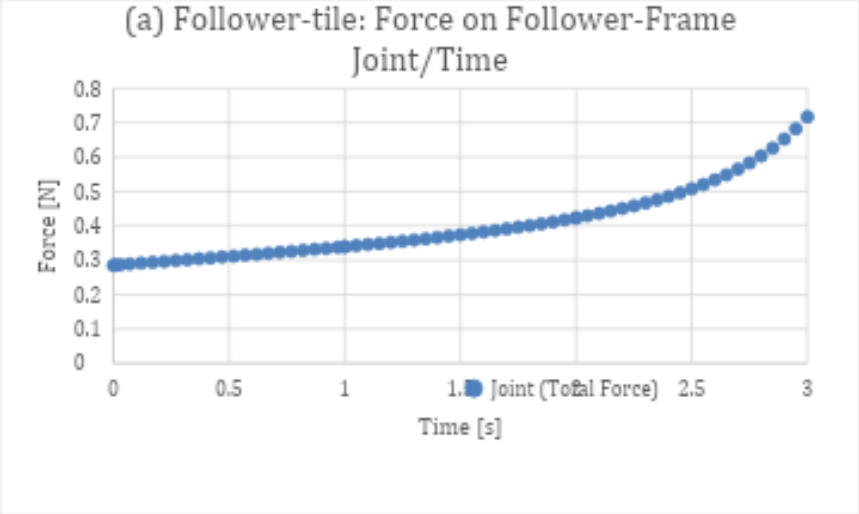

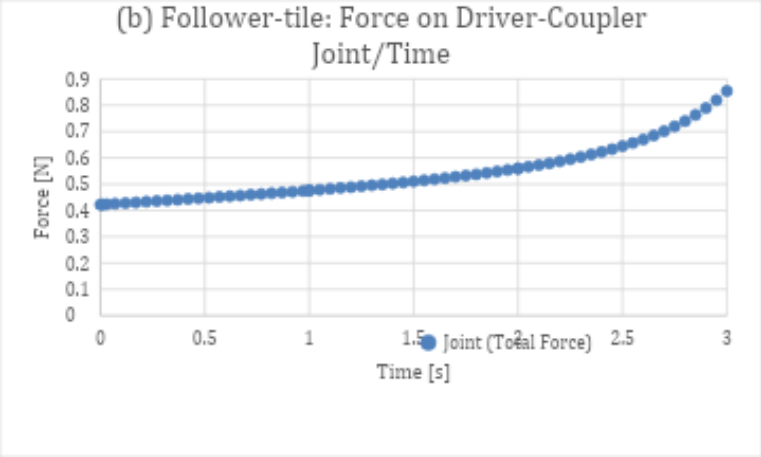

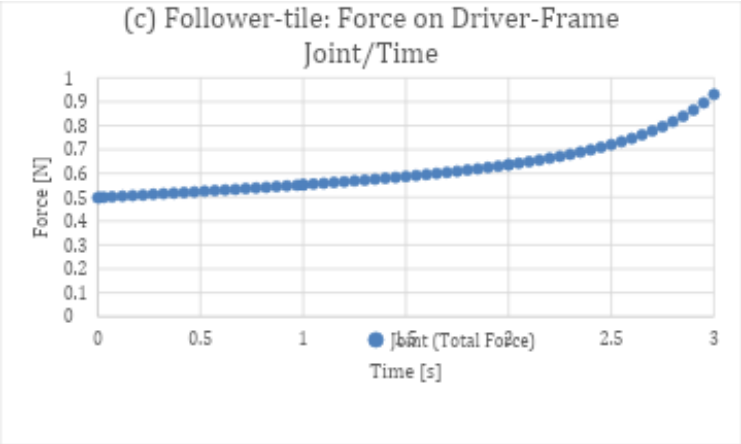

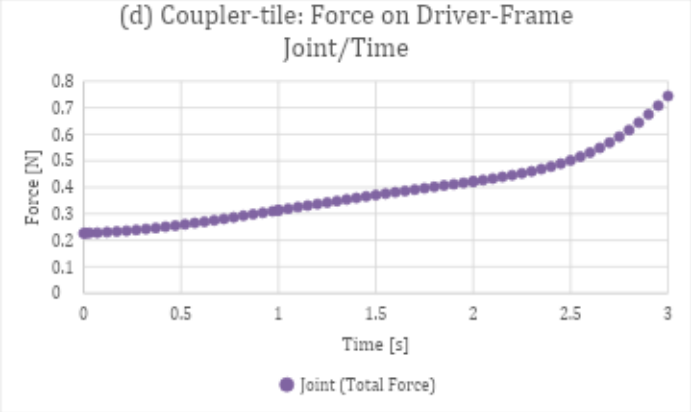

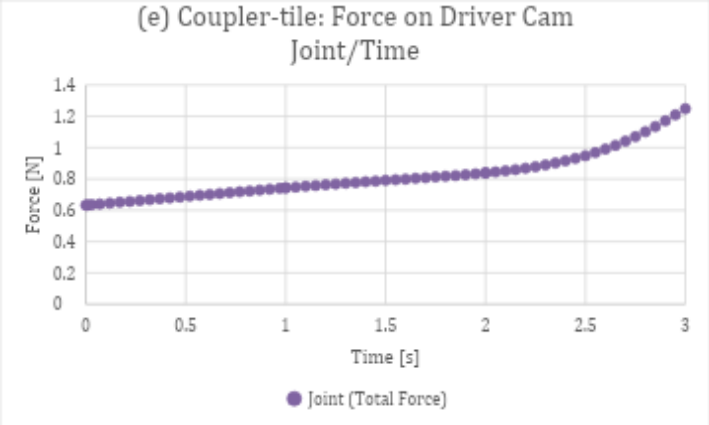

Figure 10 shows reaction forces at the mechanism joints as a function of time. ***(a)*** *Force on the follower-frame joint of the Follower-tile configuration.* ***(b)*** *Force on the driver-coupler joint of the*

Follower-tile configuration. ***(c)*** *Force on the driver-frame joint of the Follower-tile configuration.* ***(d)*** *Force on the driver-frame joint of the Coupler-tile configuration.* ***(e)*** *Force on the driver cam joint of the Coupler-tile configuration.*

All of these joints show a consistent load increase without any sharp spikes while nearing the end of the tile's opening movement. The forces on the driver-coupler and the driver-frame joints of the follower-tile peak at around 0.9 N *(b and c)*, both increasing by 0.4 N. The follower-frame joint reaches 0.7 N with the same increase of 0.4 N *(a)*.

The driver-frame and the driver cam joints of the coupler-tile experience a force increase of 5.5 and 6 N, respectively *(d and e)*. While the maximum force on the driver frame is 0.75 N at 3 s, the force on the driver cam joint measures a maximum of 1.2 N, the highest of the gradual and constant increasing forces on the joints.

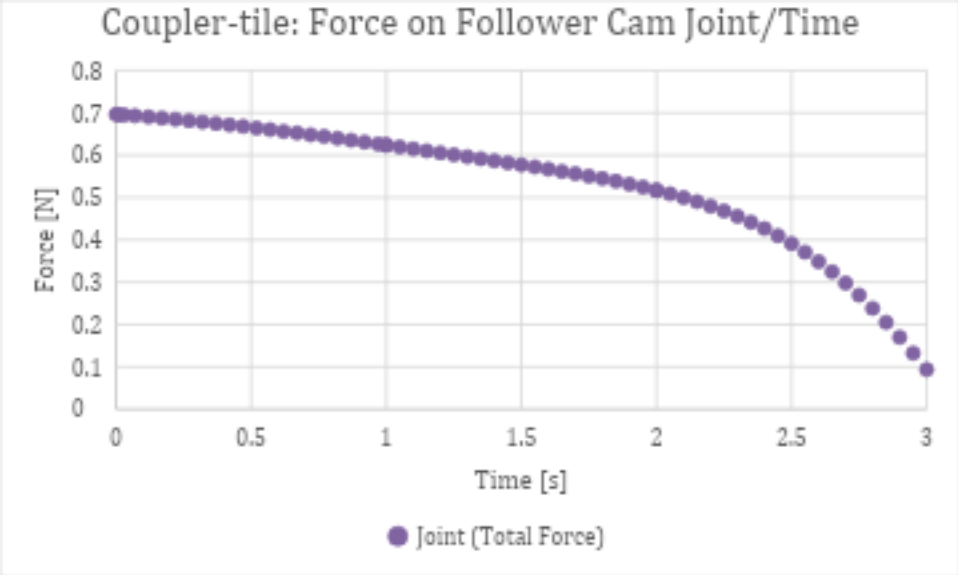

Figure 11 illustrates the reaction force on the follower cam joint of the Coupler-tile configuration as a function of time.

Contrarily, the follower cam joint is subjected to 0.7 N at the initial position; the force then smoothly lessening to 0.1 N *(Figure 11)*.

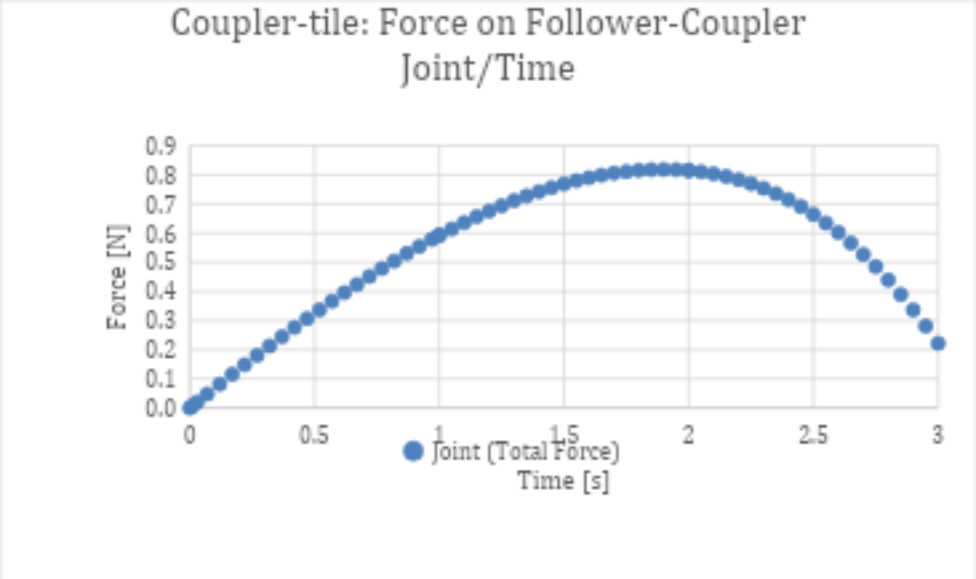

Figure 12 presents the reaction force on the follower-coupler joint of the Coupler-tile configuration as a function of time.

The force on the follower-coupler joint increases to 0.8 N from 0 N in the first 2 s, then declining to 0.2 N during the dwelling period of the cam *(Figure 12)*.

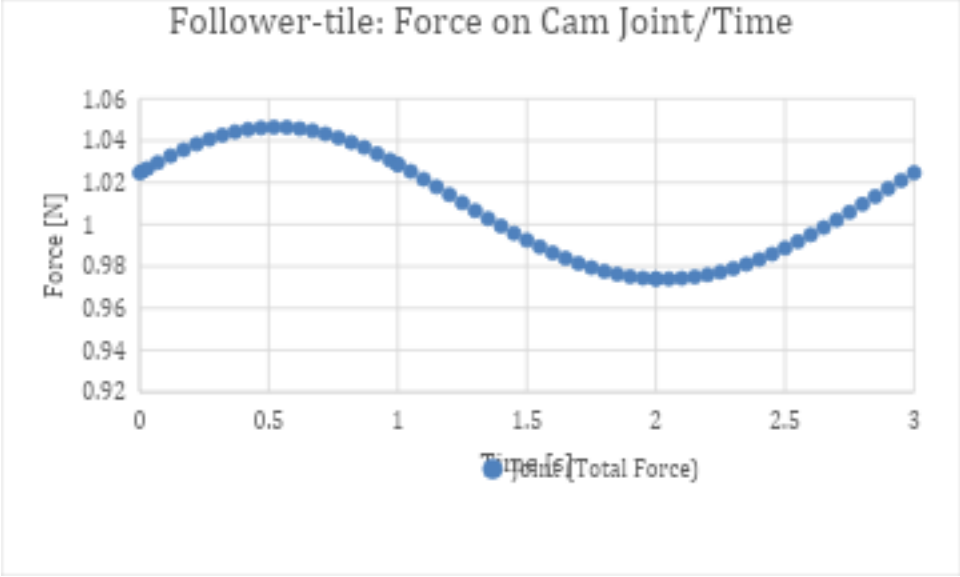

Figure 13 shows the reaction force on the cam joint of the Follower-tile configuration as a function of time.

The periodic nature of a cam is apparent on the cam of the follower-tile, and the force decreases whenever the weight of the mechanisms aligns with the camshaft axis. The amplitude of this oscillation is 0.036 N with an equilibrium point of 1.01 N. Therefore, as seen on the graph, the maximum value of the force is 1.046 N while the minimum is 0.974 N *(Figure 13)*.

RESULTS

a) Position

From **(a)** of *Figure 6*, it can be observed that the centre of mass of the follower-tile experiences a total positional variation of approximately 1.5 cm. Despite the cam lifting the overall structure, the Z-component decreases, indicating that the centre of mass is lowered. This behaviour results from the edge of the tile lowering during motion, counteracting the rising motion. Meanwhile, the Y-position increases, which can be attributed to the tilting variations that occurs.

In comparison to the follower-tile, the coupler-tile *(**(b)** of Figure 6)* shows a smaller overall positional variation, measuring approximately 0.9 cm. Similar to the follower-tile, there is a decrease in the Z-component, meaning that even though the cam raises the structure, the combined tilting and lowering of the driver cause the centre of mass of the coupler-tile to drop.

Additionally, the Y-position initially increases until around 1.8 seconds, after which it begins to decrease. This behaviour results from the followers angling away from the drivers briefly before the drivers' tilt motion pulls them back toward a more vertical position.

From **(a)** of *Figure 7*, which presents the edge position of the follower-tile, the Z-position decreases sharply, as this part experiences the greatest displacement to allow the opening of the tile. Meanwhile, the Y-position also increases significantly, due to the swinging motion of the tile's edge nearing it to the frame. Overall, this results in a total positional variation of approximately 3 cm.

For the coupler-tile's edge position *(**(b)** of Figure 7)*, a similar pattern is observed: the Z-component decreases noticeably, while the Y-component increases, again due to the more pronounced swinging motion experienced at the edge compared to the centre of mass. The total positional variation here is likewise around 3 cm.

b) Velocity

As observed in **(a)** of *Figure 8* , since the Z-component of the position decreases, the centre of mass of the follower-tile exhibits a negative velocity in the Z-direction, indicating a downward acceleration. The Y-component of the velocity is initially negative, caused by the handles of the follower. These protrusions that are necessary for the secure connection, and the extra length of the protrusion between the follower and the frame cause the centre of mass to deviate slightly toward the couplers at the beginning of the motion. After this effect subsides, the velocity increases until reaching 0.5 cm/s.

For the coupler-tile's centre of mass ***((b)** of Figure 8)*, the Z-component of velocity is negative, primarily due to the tile lowering caused by its tilt, which partially cancels out the follower cam's lift, and also because of the driver cam lowering a side of the structure. The Y-component of velocity initially starts positive but eventually turns negative. This behaviour arises from the follower's small outward tilt, which creates a positive Y-velocity, and then as the driver pulls the tile and creates the tilt, the follower becomes vertical once more. Thus, the centre of mass moves left, producing a negative Y-velocity.

Examining the edge of the follower-tile ***((c)** of Figure 8)*, the Z-velocity remains negative, while the Y-velocity increases significantly due to the larger distance travelled by the edge, resulting in an almost constant velocity with minor oscillations.

For the coupler-tile's edge velocity ***((d)** of Figure 8)*, the Z-component remains negative, also reflecting the downward motion at the tile's opening. Along the Y axis, the motion of the edge could be likened to the reflection of a circular movement around the coupler-follower joint. This would mean that during the first phases of the movement, the velocity should be low, accelerating towards the end. Yet this is not the case, the Y-component staying nearly constant. This is due to the tilt the followers experience, being tilted outward initially, increasing speed. Later, they swing back toward the drivers and become vertical once again, pushing the edge towards the left. The culmination of these movements results in an almost constant velocity. In the end, the total velocity experiences constant acceleration.

c) Acceleration

The centre of mass and edge ***((a)** and **(b)** **of** Figure 9)* of the follower-tile show very similar trends because of their alignment. However, the edge experiences larger displacements, resulting in higher acceleration values overall. Interestingly, the lowest acceleration of the Z-component of the centre of mass is lower than that of the edge. This can be attributed to the fact that while the edge experiences a greater downward velocity, the effects of the raise by the cam are more pronounced at the centre because of this. Therefore, after the speed caused by the cam subsides nearing the middle, the centre experiences a greater acceleration.

For the coupler-tile, the acceleration increases toward the end of the motion. This occurs because the driver completes its motion, causing the leaned-back frame to realign itself with the z-axis, resulting in the largest movement at the end. The centre of mass ***((c)** of Figure 9)* experiences an acceleration toward the ground due to the tilt and the realignment of the followers, and an acceleration toward the left as the realignment pushes the tile.

However, the Y-component of acceleration of its edge increases ***((d)** of Figure 9)*. This is because of the motion of the topmost part of the tile toward the left, causing the edge to move to the right. The Z-component is negative, as the edge also accelerates towards the ground.

d) Joint Forces

For the follower-tile, the forces on the follower-frame, driver-coupler, and driver-frame increase as the tile moves toward a more vertical position ***((a), (b)** and **(c)** of Figure 10)*. This increase occurs because the acceleration of the tile toward the ground amplifies the load that the joints must support.

For the coupler-tile, the driver-frame ***((d)** of Figure 10)* joint sees an increase in load because the driver and driver frame move out of alignment, which raises torque and load bearing. Additionally, the driver cam joint force ***((e)** of Figure 10)* rises because, initially, the cam shaft, driver, driver frame, and cam centre are aligned. As the simulation progresses and the cam lowers the tile, the cam centre goes out of line, which increases the torque on the joint. One other reason is that the cam's motion causes more movement along the Z axis as the simulation nears its end and the cam centre-cam line becomes perpendicular with driver frame base-cam line.

The force on the follower cam joint *(Figure 11)* decreases compared to its great initial value. This is because at the initial position, the cam centre, cam shaft, and follower frame are at the position furthest from alignment. As the cam lifts the tile, these components become increasingly more aligned, which reduces torque and therefore lowers the force.

For the follower-coupler joint *(Figure 12)*, the slight backward lean of the follower causes it to go out of alignment with its centre, generating torque. Much of the tile's load is carried by this joint because the opposite side of the tile lowers. As the motion progresses, the backward lean is corrected, reducing the force, though it does not drop entirely, since the coupler-driver joint still carries a smaller portion of the load.

Finally, regarding the follower-tile's cam joint *(Figure 13)*, the force oscillates. This occurs because as the cam centre moves out of line with the cam shaft and frame, the force increases, and as alignment improves, the force decreases with the reduction in torque. At the end of the 3 seconds, during the dwelling period, the force rises again as the cam centre shifts out of line, requiring applied force to maintain the current position.

DISCUSSION

Based on the quantitative data gathered, and the following interpretations, several observations can be made. The lack of any spikes or reversals in the position graphs *(Figures 6 and 7)* indicates the designs' efficiency. The retrieved results are in accordance with the intended motions, and therefore the modelling aspect is considered a success.

The velocity graphs *(Figure 8)* consolidate that the designs showed proper behaviour. While lack of spikes and conflicting data indicates reliability, the high velocities at the end of the simulations point to necessary improvements. The assignment of constant angular velocities was done to simplify the simulations' load. However, this caused unnecessary speed to remain at the end of the motion, which will lead to an impact between the mechanical parts. The crash will decrease the longevity and lower the efficiency.

This can further be seen from the acceleration graphs *(Figures 9)*. As mentioned before, because the closing of the tiles will mirror that of the opening, the remaining acceleration will either result in the aforementioned impact or the relatively great requirements of force to counteract the final accelerations.

Although this simplification of using a constant angular velocity rather than realistic acceleration and deceleration profiles, the resulting joint load graphs *(Figures 10-13)* remained smooth and free of spikes. This consistency and the well-coordinated movements shown in the position graphs suggest that, with correctly applied motion parameters, the mechanisms could operate without collisions or energy waste.

Additionally, the necessary electrical circuits and servo motors required to actuate the structure were excluded from the analysed models. The servos, designed to be placed on the cam and driver-frame joints, face significant dimensional constrains given the tight clearances between bodies. Consequently, predicting the longevity of these servos and their battery lives require simulating or manufacturing the entire board to acquire comprehensive data.

Future research must also address the replacement methods for the power sources of servos and the retrieval of the pieces after a game. This research has focused on individual tiles, therefore a robotic arm-driven automated chessboard equipped with these models would necessitate reopening each tile to collect the pieces, assuming enough space for the pieces to remain vertical exists inside the board. Under the same assumption, piece retrieval in a slider-based system could be automated by sliding the pieces beneath the board to an opening where they can be lifted back onto the surface at the end of the game. A simple pulley system actuated by a servo would suffice, as the pieces can be positioned onto and off the lift by the slider.

Furthermore, the differing designs could have different uses. The simplicity of the follower-tile design would greatly reduce 3D printing or manufacturing costs. Moreover, the greater amount of tilt of this design would indicate to higher reliability. The constantly high and oscillating force on its cam joint and the increased load on the driver-coupler joint could limit its longevity, requiring more replacements. However, it is cheaper and more compact in return.

The more complex and larger coupler-tile design would be harder to produce, and the intricate parts would render this harder to replace. However, this design could be modified to a greater extent as the driver and follower frames have many possibilities of improvements and changes.

The integration of these novel designs requires further planning and real-life testing. While these designs increase the mechanical complexity of the existing automated chessboards, they offer a critical trade-off by significantly lowering energy requirements and capture durations. Furthermore, while the integration with a robotic arm-driven system is relatively straightforward as the arm operates above the board, the integration with a slider-based mechanism presents complications. It necessitates the avoidance of ferromagnetic materials in the structure, and the recalibration of magnetic forces to account for the electromagnetic interference caused by the servo motors.

The material selection is also crucial for the longevity of the designs and the energy efficiency. The default material used for the simulation was stainless steel. This gave excellent structural durability (Young's Modulus: 190-210 GPa) to the design. However, its high density caused elevated joint force values in the gathered graphs. Manufacturing the machine parts from wood would significantly reduce weight, therefore reducing the load on servos and increasing their lifespan. While the loadbearing capacity of hardwoods like oak are still high (Young's Modulus of oak: 11-12 GPa), wood is anisotropic

and weak against environmental conditions. This would reduce precision, as circular movements could deform the parts, and the board would be weak against environmental factors such as humidity. Alternatively, thermoplastics used in 3D printing offer a lightweight, low-cost and humidity-resistant solution. However, plastics suffer from creep and have lower stiffness (Young's Modulus: 2-3 GPa), a plastic design could cause long-term precision issues under the constant load of the pieces.

In addition to the mentioned improvements of better and more realistic motion definitions and design changes, the employment of different mechanical linkages could be explored.

This study is positioned as a simulation-based proof of concept. A prototype was not fabricated due to lack of in-house fabrication capability within the program timeline. Future work will incorporate friction considerations, the mentioned material selections and fabrication when facilities are available.

CONCLUSION

The purpose of this study was to offer new capture-dedicated mechanisms to chess automation systems with the aim of lessening capture move durations. The current automated chess games employ the same mechanism for piece captures and movements. The models in this paper work separately from the piece movement mechanisms, removing the captured piece while the capturing piece is being moved. This shortens the duration of capture moves drastically, requiring less computation and displacement from the piece movement mechanism. The piece capture mechanisms' simplicity relative to the movement mechanisms renders the capture move more reliable by minimising the number of potential failure points. These two designs were created to fit under each tile, capable of opening to let the captured piece fall into the chessboard to be collected at the end of the match. The two designs were analysed, comparing positional, velocity, acceleration, and joint force graphs on key points. The follower-tile design was concluded to have greater mobility while possessing fewer parts. The coupler-tile design was concluded to have improved longevity compared to the follower-tile, having lower overall forces on its joints. However, the increased complexity was a drawback. By successfully achieving the intended tilt in the ANSYS Mechanical simulation environment, both designs demonstrate that mechanical components can virtually eliminate the computational load required by robotic arm-driven or slider-based mechanisms, which otherwise necessitate extra path-planning for capture moves.

These new models could be better analysed by running more accurate simulations, better regulating the angular velocities of joints. A complete chessboard could also be simulated in order to better contextualise the findings. The omitted frictions and mechanism materials could be taken into consideration to simulate the products with higher accuracy. Lastly, different cam profiles could be utilised to get a specific rise and fall sequence.

REFERENCES

[1] F. Y. Ómarsdóttir, R. B. Ólafsson, and J. T. Foley, "The Axiomatic Design of Chessmate: A Chess-playing Robot," in *Procedia CIRP*, Elsevier B.V., 2016, pp. 231–236. doi: 10.1016/j.procir.2016.07.002.

[2] T. D. Phuc and B. C. Son, "Development of an autonomous chess robot system using computer vision and deep learning," *Results in Engineering*, vol. 25, Mar. 2025, doi: 10.1016/j.rineng.2025.104091.

[3] K. Shin *et al.*, "Exploring the Capabilities of a General-Purpose Robotic Arm in Chess Gameplay," in *IEEE-RAS International Conference on Humanoid Robots*, IEEE Computer Society, 2023. doi: 10.1109/Humanoids57100.2023.10375209.

[4] R. Zhang, J. de Winter, D. Dodou, H. Seyffert, and Y. B. Eisma, "An open-source reproducible chess robot for human-robot interaction research," *Front Robot AI*, vol. 12, 2025, doi: 10.3389/frobt.2025.1436674.

[5] C. Jariyavajee, A. Visavakitcharoen, P. Sirimaha, B. Sirinaovakul, and J. Polvichai, *A Practical Interactive Chess Board with Automatic Movement Control*. [IEEE], 2018.

[6] S. Sarker, "Wizard Chess: An Autonomous Chess Playing Robot."

[7] A. Thabet and J. Prasetyo, "Design and Implementation of a Smart Automated Chess Board," *Journal of Applied Science and Advanced Engineering*, vol. 3, no. 2, pp. 64–72, Sep. 2025, doi: 10.59097/jasae.v3i2.52.

[8] Pendo Technology Limited, "Chessnut Move Advanced Robotic Chessboard." Accessed: Nov. 28, 2025. [Online]. Available: https://www.chessnutech.com/pages/chessnut-move

[9] S. R. Kashef, S. Amini, and A. Akbarzadeh, "Robotic hand: A review on linkage-driven finger mechanisms of prosthetic hands and evaluation of the performance criteria," Mar. 01, 2020, *Elsevier Ltd*. doi: 10.1016/j.mechmachtheory.2019.103677.

[10] Q. T. Truong, Q. V. Nguyen, H. C. Park, D. Y. Byun, and N. S. Goo, "Modification of a four-bar linkage system for a higher optimal flapping frequency," *J Intell Mater Syst Struct*, vol. 22, no. 1, pp. 59–66, Jan. 2011, doi: 10.1177/1045389X10392611.

[11] M. R. Mali, P. D. Maskar, S. H. Gawande, and J. S. Bagi, "Design Optimization of Cam & Follower Mechanism of an Internal Combustion Engine for Improving the Engine Efficiency," *Modern Mechanical Engineering*, vol. 02, no. 03, pp. 114–119, 2012, doi: 10.4236/mme.2012.23014.

[12] R. D. V. Prasad, K. Satyanarayana, Ch. Maheswara Rao, and M. S. S. Srinivas Rao, "Analysis of Cam and Follower Mechanism to Reduce Jerk and Induced Stresses," *Journal of Recent Trends in Mechanics*, vol. 5, no. 3, pp. 8–17, Dec. 2020, doi: 10.46610/jortm.2020.v05i03.002.